Environmental Oxygen Regulates Astrocyte Proliferation to Guide Angiogenesis during Retinal Development

Robin M Perelli[1,2,*], Matthew L O'Sullivan[2,3,*], Samantha Zarnick[1,2], and Jeremy N Kay[1,2,]

1) Department of Neurobiology; 2) Department of Ophthalmology; 3) Ophthalmology Residency Program, Duke University School of Medicine, Durham, North Carolina 27710

*These authors contributed equally to this work.

Correspondence to:

Jeremy Kay

Duke Eye Center

Box 3802

Durham, NC 27710

jeremy.kay@duke.edu

Abstract

Transient neonatal exposure to high oxygen levels is a major risk factor for retinopathy of prematurity (ROP), a disease of perturbed retinal vascular development. The factors that interrupt normal angiogenesis following oxygen exposure remain unclear. Formation of retinal vasculature requires guidance cues from astrocytes, suggesting that astrocyte disruptions could contribute to oxygen-induced retinopathy. However, it is presently unknown whether environmental oxygen influences formation of the angiogenic astrocyte template. To investigate this question we raised neonatal mice in hyperoxic conditions (75% O_2) from postnatal day 0-4, when the astrocyte pattern is being established. We found that hyperoxia suppressed astrocyte proliferation, whereas return to room air at P4 induced a major astrocyte proliferative response, massively increasing astrocyte numbers and disturbing their spatial patterning prior to arrival of developing vasculature. This treatment paradigm also disrupted vascular development in a manner reminiscent of ROP, leading to vitreous hemorrhage and neuroretina defects. Moreover, within individual animals, the severity of vascular phenotypes was strongly correlated with the number of excess astrocytes. Direct exposure to hypoxia (10% O_2) produced similar effects, indicating that developing astrocytes are sensitive to relative decrements in oxygen availability. Molecular analysis revealed that the proliferative response was blunted in mice bearing an astrocyte-specific ablation of the HIF2α transcription factor. Together, our results support a model in which neonatal astrocytes use a HIF2α-dependent pathway to sense oxygen levels, thereby regulating the number of astrocytes within the angiogenic template. In this model, fluctuations in environmental oxygen can become pathogenic when they over-stimulate this proliferation control mechanism, leading to excess astrocytes that interfere with retinal angiogenesis.

Introduction

Precise coordination between growing neurons, glia, and blood vessels is a central feature of neural development and is essential for building a functional nervous system. A striking example of coordinated neuro-glial-vascular growth occurs in mammalian retina, within a structure known as the retinal nerve fiber layer (RNFL). This layer, which sits at the vitreal surface, contains several different structures that are essential for visual function. These include the intrinsic retinal vasculature; the retinal ganglion cell (RGC) axons, which course through this layer on the way to the optic nerve head; and a population of glia known as RNFL astrocytes. During development, astrocytes and blood vessels invade the retina through the optic nerve head and spread centrifugally through the RNFL to colonize the entire retinal surface (Selvam et al., 2018). These migratory events are coordinated through an intricate series of cell-cell interactions: RGC axons play an instructive role in guiding astrocyte migration, and astrocytes in turn form a template that guides the vasculature during angiogenesis (Dorrell et al., 2002; Fruttiger et al., 1996; Gerhardt et al., 2003; O'Sullivan et al., 2017). When this sequence of events is disrupted, there are major deleterious consequences for retinal angiogenesis. For example, developmental vascular disorders such as retinopathy of prematurity (ROP) are marked by delay or arrest of the RNFL angiogenic wavefront (Foos, 1987; Hellström et al., 2013). It is therefore of great interest to understand the developmental mechanisms that enable the orderly progression of retinal angiogenesis and how they might become perturbed in the context of ROP pathology.

The principal risk factors for ROP are prematurity, low birth weight, and supplemental oxygen. In infants affected by ROP, halted extension of nascent vessels leaves the peripheral retina avascular (Foos, 1987). This is commonly termed Phase 1 of ROP. Subsequently, in Phase 2, hypoxia in the ischemic peripheral neuroretina stimulates uncontrolled neovascularization, which can progress to preretinal fibrovascular proliferation and ultimately retinal detachment (Hellström et al., 2013). Exposure to oxygen is thought to be a key ROP risk factor because hyperoxia diminishes the molecular drive for angiogenesis. As such, hyperoxia could explain the wavefront arrest. However, it remains unclear why vessels do not resume their orderly progression through the RNFL once normoxic conditions are restored.

One possible explanation for this failure of wavefront progression is that the astrocytic template for angiogenesis becomes disturbed. In normal development, astrocytes arrange their somata and arbors into a pre-pattern resembling a capillary bed. This astrocyte template exerts powerful effects on the ultimate pattern of the vascular network, and is required for normal vascular morphogenesis (Fruttiger et al., 1996; Gerhardt et al., 2003; O'Sullivan et al., 2017; Tao and Zhang, 2016). Despite this

well-established role of astrocytes in RNFL vascular development, the role astrocytes play in ROP remains obscure. ROP histopathological studies have noted that the fibrovascular ridge – a pathological structure that forms at the junction between vascular central and avascular peripheral retina – is composed predominately of astrocytes, whereas few astrocytes are detected peripheral to this ridge (Sun et al., 2010). Thus, there is reason to think that astrocyte patterning might be disturbed in ROP. However, despite some hints from animal studies (Morita et al., 2016; Zhang et al., 1999), it is presently unknown whether astrocyte development is impacted by ROP risk factors such as hyperoxia. Resolving this issue has the potential to reveal new developmental mechanisms regulating normal astrocyte development, and would clarify whether altered astrocyte development is a plausible candidate to underlie ROP vascular pathology.

To investigate these questions, we sought to understand astrocyte development in a mouse model of oxygen-induced retinopathy (OIR). Since the identification of oxygen as the major modifiable risk factor for ROP, several animal OIR models have been developed. In the most common model, mouse pups are exposed to 75% O_2 from postnatal day 7 (P7) to P12 (Smith et al., 1994). This manipulation causes central capillary vaso-obliteration during the period of hyperoxia followed by neovascularization upon return to room air. This paradigm has proven to be a powerful tool for exploring molecular mechanisms of neovascularization and oxygen toxicity. However, it has some limitations, particularly as a model of Stage 1 ROP. First, the phenotype of mouse OIR – central vaso-obliteration and neovascularization – does not model the peripheral avascularity seen in ROP, nor the hyperplasia at the vascular-avascular junction (Foos, 1987). Second, the P7 onset of oxygen manipulation is after the majority of astrocyte development is complete and primary vascular plexus has been established, which places the physiologic insult at a later ontogenetic stage than ROP. For these reasons, we explored the possibility of starting hyperoxia exposure at earlier stages. Unlike in standard OIR, a period of hyperoxia at P0 can cause long-term retinal vascular pathology with features reminiscent of advanced ROP (Lajko et al., 2016; McMenamin et al., 2016). Thus, mouse models featuring early hyperoxia may have utility in understanding Phase 1 of ROP and the involvement of astrocytes. However, other studies have reported minimal long-lasting vascular effects following P0 hyperoxia (Morita et al., 2016), so the extent to which this paradigm serves as a useful disease model remains uncertain.

Here we show that neonatal exposure to hyperoxia has long-lasting consequences for development of RNFL astrocytes and vasculature. In our protocol, mice were raised in hyperoxic conditions starting at P0 and returned to room air at P4. Retinal defects including vitreous hemorrhage

and retinal degenerative changes persist for weeks after return to normoxia. To understand the origin of these defects we examined development of vasculature and astrocytes in this model. Consistent with previous reports (Morita et al., 2016; West et al., 2005), we found that the hyperoxic phase of the protocol prevents retinal angiogenesis while permitting astrocyte migration. Return to normoxia triggered a surge in astrocyte mitotic activity producing a vast excess of astrocytes at an age when the astrocyte population normally dwindles. Environmental hypoxia similarly stimulates astrocyte proliferation, suggesting that a relative decrease in oxygen levels is the mitogenic stimulus. Astrocyte proliferation following hyperoxia was blunted by cell-type specific knockout of HIF2α, indicating that oxygen-sensitive transcriptional programs intrinsic to astrocytes regulate their mitotic activity. Following the initial proliferative response, the severity of persistent astrocyte defects was variable between animals. Strikingly, the severity of vascular defects was strongly correlated with the severity of the excess astrocyte phenotype. We propose a model in which the number of retinal astrocytes is modulated by oxygen through HIF2α, and that dysregulation of this pathway perturbs formation of the angiogenic astrocyte template leading to defective angiogenesis.

Methods

Mice

All experiments were conducted with the approval and under the supervision of the Due Universty IACUC. For experiments with wild type mice, timed pregnant CD1 mice were purchased from Charles River (Wilmington, MA). GFAP:Cre with the human GFAP promoter driving expression of Cre recombinase (Zhuo et al., 2001) were acquired from Jackson Laboratory (Jax stock 004600). Cre-conditional HIF2α mice (Gruber et al., 2007) were also acquired from Jackson Laboratory (Jax stock 008407). For experiments with CD-1 mice, pups from 2-4 litters were randomly assorted and cross-fostered amongst the 2-4 mothers in the experimental cohort to control for effects of litter and variation in birthdating.

Environmental oxygen manipulation

Cages with litters of mice and their mothers were placed inside an environmental chamber (A15274P, BioSpherix) to regulate oxygen concentrations. Medical O_2 or N_2 was mixed with room air by a regulator and O_2 concentration calibrated and monitored with an O_2 sensor (ProOx Model 360, BioSpherix). 75% O_2 was used for hyperoxia and 10% O_2 for hypoxia.

Immunohistochemistry

Mice were anesthetized with ice or isoflurane, rapidly decapitated, eyes removed and immersion fixed in 4% paraformaldehyde for 1.5 hours at 4°C before being stored in phosphate buffered saline (PBS) at 4°C. Retinas were dissected free from the fixed eyes and blocked at room temperature for 1 hour in PBS with 0.03% Triton X-100 (Sigma-Aldrich) and 3% Normal Donkey Serum (Jackson Immunoresearch). Retinas were then stained with primary antibody for 5-7 days at 4°C, washed 3 times with PBS, and then stained with donkey secondary antibodies (Jackson Immunoresearch) at a standard dilution of 1:1,000. Following immunostaining, 4 relieving cuts were made in the retinas and they were flat-mounted on cellulose membranes (Millipore HABG01300) on glass slides and coverslipped with Fluoromount-G (Southern Biotech).

For cryosections, fixed whole eyes were sunk in 30% sucrose in PBS overnight. 20 μm sections were then cut using a cryostat. Sections were hydrated for 10 minutes with PBS and blocked for 30 minutes in PBS with 0.03% Triton X-100 (Sigma-Aldrich) and 3% Normal Donkey Serum (Jackson Immunoresearch). Sections were incubated in primary antibodies overnight, washed three times with PBS, stained with secondary antibodies for two hours, and washed twice with PBS before mounting with Fluoromount-G.

Primary antibodies used were as follows: goat anti-GFAP (1:1,000, Abcam ab53554); rat anti-Ki67 (1:3,000, Ebioscience 14-5698-80); mouse anti-neurofilament (1:1,000, EMD Millipore MAB1621); rabbit anti-Pax2 (1:200, Covance PRB-276P); rat anti-PDGFRa (1:100, BD Biosciences 558774); rabbit anti-Sox9 (1:4,000, Millipore AB5535); goat anti-VEGF-A (R&D Systems, AF-493-SP); Griffonia simplicifolia Isolectin B4 (IB4; 1:100, Life Technologies; Alexa 488- conjugated I21411, or biotinylated I21414) was included with primary antibodies to stain blood vessels.

Microscopy and image analysis

Retinas were imaged on a Nikon A1R confocal laser scanning microscope with 4x air, 20x air or 60x oil immersion objective lenses. A resonant scanner and motorized stage were used to acquire whole-retina tile scan images. Images were then processed and analyzed in FIJI/ImageJ (Schindelin et al., 2012). Sox9 and Sox9/Ki67 double positive astrocytes were counted manually in 60x images. Total astrocyte numbers were estimated by multiplying retina area by average weighted astrocyte density; 3-4 fields of view from central, mid-peripheral, and peripheral eccentricities were analyzed, mean density for each eccentricity in each retina calculated, and overall average density calculated by weighting

central, middle, and peripheral eccentricities with factors of 0.11, 0.33, and 0.56, respectively, based on a circular approximation of the retina divided into 3 zones by concentric rings with radii of 1x, 2x, and 3x (O'Sullivan et al., 2017). For hypoxia experiments, we found that rearing mice in 10% O2 strongly inhibited migration of astrocytes into peripheral retina. Therefore, to avoid confounding our proliferation analysis, we limited our quantification of $Ki67^+$ astrocytes to the central retinal region that astrocytes were able to colonize normally.

Astrocyte and blood vessel coverage

To assess retinal coverage by astrocytes and blood vessels, low-magnification tile-scan images of whole retinas were used. The retinal perimeter was manually traced in ImageJ to measure the area of each retina, and within that perimeter a second curve encompassing furthest peripheral Sox9 or IB4 stained area was drawn and its area measured to yield astrocyte and blood vessel area, respectively.

Data analysis

Statistical analyses were performed in GraphPad Prism 8 (GraphPad Software) or JMP Pro 13 (SAS Institute). Two-tailed T-tests and 2-way ANOVAs with post-hoc multiple comparisons by T-test with Holm-Sidak correction were used to test for statistical significance. Summary statistics reported as mean ± s.e.m., and error bars display s.e.m.

Results

Neonatal hyperoxia disrupts retinal vascular development

To investigate how early disruptions in oxygenation affect retinal vascular development, we raised newborn mice in 75% O_2 or room air (21% O_2) from P0 to P4. Vessel development was assessed during and after the hyperoxia period by staining flat-mounted retinas with the endothelial cell marker isolectin B4 (IB4), and quantifying the retinal area covered by vessels Fig. 1A,B). Hyperoxia significantly delayed progression of angiogenesis relative to normoxic controls (Fig. 1C). Indeed, consistent with prior reports (Morita et al., 2016; West et al., 2005), hyperoxia completely prevented blood vessel sprouting from the optic nerve head (ONH) with the rare exception of a few stray vessels escaping into the proximal portions of the retina. Only after the mice were returned to normoxic conditions did the primary vascular plexus begin to grow (Fig. 1B,C). The centrifugal extension of the vascular wavefront was more variable in hyperoxia-exposed mice compared to controls. Eventually, however, the vasculature was able to reach the retinal margin in all treated mice, such that the entire nerve fiber layer

was vascularized by P21 (Fig 1C). Intriguingly, hyperoxia starting at P2 or P4 after retinal angiogenesis had been initiated did not delay the peripheral extension of the vascular wavefront, but instead resulted in central capillary loss more reminiscent of the widely used mouse OIR paradigm (Supplemental Fig. S1). Together, these observations suggest that hyperoxia delays the onset of angiogenesis but does not prevent its completion.

A close examination of the vascular phenotypes in hyperoxia-treated mice revealed that angiogenesis was not just delayed but also dysfunctional. We noted three particularly striking vascular abnormalities. First, about half of the eyes from P12 and older mice had conspicuous vitreous hemorrhages (Fig. 2A,B), which was never seen in controls. The presence of vitreous hemorrhage was also correlated with the severity of vascular delay at P12, such that eyes with bleeding had retinas with greater delays in vascular coverage (Fig. 2B). Second, the hyaloid system of hyperoxia treated eyes failed to regress. Dense hyaloid vessels were evident throughout the vitreous during dissection, the hyaloid artery could be seen emerging from the optic nerve head (Fig. 2C), and IB4-positive vascular tissue originating from the hyaloid vessels was present circumferentially in the peripheral retina (Fig. 2D). Third, all treated retinas, regardless of vessel coverage delay, exhibited abnormal vascular morphology: The radial organization of large vessels was usually absent; capillaries were of abnormally large caliber; and endothelial cells frequently formed lawns without any evident tubular structure (Fig. 2D,E). Moreover, vessel network organization was haphazard, with increased vessel tortuosity and smaller capillary loops (Fig. 2D,E). Overall, these experiments demonstrate that neonatal hyperoxia not only delays angiogenesis but also causes vascular pathology in the developing mouse retina. Our results therefore establish the P0-P4 hyperoxia protocol as a neonatal oxygen induced retinopathy (NOIR) paradigm.

Hyperoxia suppresses and return to normoxia stimulates astrocyte proliferation

We next used the NOIR protocol to examine the effects of oxygen treatment on developing astrocytes. The hyperoxic phase of the protocol – i.e. P0-P4 – corresponds to the period when astrocytes are normally migrating to colonize the retinal periphery (Chan-Ling et al., 2009; Fruttiger, 2002; O'Sullivan et al., 2017). However, migration was unaffected by hyperoxia: astrocytes spread outward from the ONH to cover the retina, associated with RGC axons, and became polarized along the centrifugal axis similarly in normoxic and hyperoxic conditions (data not shown). Accordingly, total astrocyte number was normal in treated mice at the conclusion of the hyperoxic phase (Fig. 3B). Thus,

the aforementioned delay in angiogenesis (Fig. 2) was not due to impairment in astrocyte colonization of the retina during the P0-P4 period.

Because the astrocyte template was largely unaffected by hyperoxia, we next investigated whether the hypoxic stress associated with the return to room air might perturb astrocyte development. Whole-mount staining for astrocyte nuclear markers revealed that, four days after return to room air, treated mice exhibit an obvious and major increase in astrocyte numbers (Fig. 3A). In wild-type mice, astrocyte numbers normally increase until P5-6 due to ongoing migration and proliferation; subsequently, their numbers decline substantially due to cell death (Chan-Ling et al., 2009; Puñal et al., 2019). A similar pattern was observed in our control normoxia mice (Fig. 3B). By contrast, in treated mice the number of astrocytes began to dramatically increase starting at P6, during the time when the astrocyte population was dwindling in controls (Fig. 3A,B). The increase in astrocyte numbers persisted for weeks – in some cases as long as P21 (Fig. 3B).

Given these large differences in astrocyte numbers, we surmised that astrocyte mitotic activity might be regulated by oxygen. To test this idea, we used Ki67 as an immunohistochemical marker of dividing cells (Fig. 3C). In normoxic controls, the fraction of $Sox9^{+}Ki67^{+}$ proliferative astrocytes decreased monotonically over development, such that virtually all astrocytes were quiescent by P10 (Fig. 3D). By contrast, in mice exposed to the NOIR protocol, astrocyte proliferation was regulated in a triphasic manner: Initially, during the hyperoxic phase, astrocyte proliferation was suppressed relative to controls; the return to room air then stimulated increased rates of proliferation at P6 and P8 before mitotic activity ultimately fell to control levels (Fig. 3C,D). Importantly, the increase in proliferative astrocytes at P6 preceded the increase in astrocyte number at P8, suggesting that proliferation likely accounts for the expansion of the astrocyte population. These findings are consistent with a model whereby return to room air at P4 stimulates astrocyte proliferation, thereby elevating astrocyte numbers in NOIR mice. The proliferative response appears to be quite reliable across mice, as both the surge in proliferation at P6 (Fig. 3D) and the surge in astrocyte abundance at P8 (Fig. 3B) were highly consistent between animals. Subsequent factors affecting astrocyte number, by contrast, appear to vary substantially between individual mice, given the wide range in astrocyte numbers that emerges by P12 (Fig. 3B,D).

Astrocyte patterning following hyperoxia is defective

The observation that astrocyte numbers are abnormal in NOIR mice raised the possibility that the angiogenic astrocyte template is disturbed by early hyperoxia. To investigate how the NOIR protocol

affects astrocyte patterning, we evaluated soma positioning and arbor anatomy in retinal whole-mounts. This analysis revealed that, in P12 treated retinas, astrocytes are arranged into irregular clumps and strands instead of being evenly spaced (Fig. 4A). The most striking effect was ahead of the vascular wavefront, where astrocyte somata were typically arranged into large honeycomb-like shapes that left large swaths of retinal territory uncovered by astrocytes or their arbors (Fig. 4A,B). Because the pattern of angiogenesis normally follows the astrocyte template, dysmorphia in the astrocyte network could be transmitted to growing vessels. Consistent with this possibility, endothelial tip cells and their filopodia at the vascular wavefront remained strictly co-localized with astrocytes in NOIR mice, even when astrocyte distribution was disturbed (Fig. 4B). Together, these findings suggest that oxygen stress alters the astrocyte template in a manner that could result in delayed or disrupted angiogenesis.

Astrocyte number predicts vascular abnormalities

The finding that neonatal hyperoxia causes both vascular and glial abnormalities spurred us to investigate whether the vascular defects might in fact originate with the glia. To this end we exploited the variability in the number of astrocytes in hyperoxia-exposed retinas at P12 (Fig. 3B). If vessel phenotypes are a consequence of astrocyte phenotypes, we would predict that the NOIR animals with the most severe astrocyte disruptions should also show the most severe vascular pathology. Consistent with this model, the total number of astrocytes was inversely correlated with vascularized retinal area, such that retinas with the greatest expansion of the astrocyte population displayed the most profound delay in peripheral extension of retinal vessels (Fig. 4C). Furthermore, animals with vitreous hemorrhage had significantly more astrocytes than those that escaped this pathology (Fig. 4D). These observations support the notion that anomalous astrocyte proliferation causes angiogenic defects in the NOIR paradigm.

Neonatal hyperoxia causes enduring retinal abnormalities

To explore the longer-term consequences that neonatal hyperoxia might hold for the retina, we examined NOIR mice and normoxic controls at three weeks of age, when the retina is largely mature. Vascular disorganization and persistent hyaloid was still evident in whole-mount NOIR retinas at P21, particularly in cases where astrocyte numbers remained high (Fig. 5C). To test for other facets of retinal pathology, retinas were cryosectioned and immunostained to assess their cytoarchitectural integrity. Hyperoxic retinas (n = 4) showed a strikingly abnormal cross-sectional profile, characterized by buckling and corrugation of the outer layers (Fig. 5A) in a manner reminiscent of ROP (Foos, 1987). This was

accompanied by large-scale reactive gliosis of Müller glia, indicated by upregulation of GFAP (Fig. 5B), which is consistent with the presence of ongoing histopathological insults or tissue stress. We also noted additional vascular phenotypes in IB4-stained sections that were not evident in the whole-mount preparations. These included laminar disorganization of the intermediate and deep vascular plexuses (Fig. 5A); intravitreal neovascularizations (Fig 5B); and hyperplastic vascular tissue at the inner retinal surface (Fig. 5A). The hyperplasic superficial vasculature was associated with a hyperplasic GFAP+ glial network, which likely included excess nerve fiber layer astrocytes as well as the endfeet of reactive Müller glia (Fig. 5B). Together, these observations indicate that a brief period of neonatal hyperoxia during a crucial period of glial-vascular development produce long-lasting deleterious consequences with features resembling ROP or other vitreoretinopathies (Eller et al., 1987; Foos, 1987; McMenamin et al., 2016).

Hypoxia stimulates astrocyte proliferation

Because neonatal hyperoxia causes long-lasting astrocyte and vascular pathology in the retina, we decided to investigate what mechanism could produce such effects. Our initial results suggested a central pathogenic role for aberrant astrocyte proliferation (Fig. 3), so we focused on learning the mechanisms that stimulate astrocyte overproduction in NOIR mice. It was clear from the NOIR experiments that exposure to high oxygen suppresses astrocyte proliferation, while return to room air promotes proliferation (Fig. 3D). These observations led us to hypothesize that the state of the cellular hypoxia-sensing machinery might directly regulate astrocyte proliferation. In this model, the cause of proliferation in the NOIR protocol is the relative hypoxia experienced by the retinal tissue upon transition from 75% to 21% oxygen. If this hypothesis is correct, then rearing mice in a hypoxic environment should mimic the proliferative effects of return to room air in the NOIR protocol. To test this idea, neonatal mice were raised in 10% O_2 from P0-4. Immunostaining with Sox9 and Ki67 revealed a striking increase in the fraction of Ki67+ proliferating astrocytes in hypoxic mice (Fig 6A,B). The effect was evident already at P2 and persisted until P4 (Fig. 6B). Consistent with this increase in proliferative astrocytes, there was also a significantly higher density of astrocytes in hypoxic retinas (Fig 6C). Indeed, by P4 astrocyte density in hypoxic retinas exceeded controls by approximately two fold (Fig. 6C). Therefore, direct hypoxia drives astrocytes to divide in a manner similar to the room-air phase of the NOIR paradigm, suggesting that a relative decrement in oxygen availability is the physiologic stimulus that drives astrocyte mitosis.

Astrocyte HIF2α is required for proliferation following hyperoxia

Finally, we investigated the molecular and cellular mechanisms underlying the detection of relative hypoxia in the NOIR paradigm. Hypoxia-inducible factors (HIFs) are crucial molecular mediators of oxygen sensing that subserve important roles in the normal development of retinal astrocytes and vasculature (Duan et al., 2014; Kurihara et al., 2010; Nakamura-Ishizu et al., 2012; Weidemann et al., 2010) . There is substantial evidence that retinal astrocytes themselves can act as oxygen sensors, using the HIF2α transcription factor as the major downstream HIF effector (Duan et al., 2014; Mowat et al., 2010; Weidemann et al., 2010). Moreover, loss of astrocytic HIF2α severely reduces retinal astrocyte numbers, suggesting it could have a role in regulating astrocyte proliferation during normal development (Duan et al., 2014). We therefore hypothesized that astrocytic HIF2α signaling might also be the key oxygen-sensitive proliferative mechanism in the pathologic NOIR context. To test this possibility we used a Cre-conditional knockout strategy, crossing *GFAP-Cre* mice (Zhuo et al., 2001) with a floxed-HIF2α mouse line (Gruber et al., 2007) to produce an astrocyte-specific HIF2α mutant (here abbreviated AC-Hif2α-KO).

We began by characterizing the efficacy of HIF2α deletion in these mutant mice. To this end we performed immunostaining for VEGF-A, a canonical direct target gene of the HIF pathway (Pagès and Pouysségur, 2005), to validate that HIF signaling was abrogated in mutant astrocytes. This analysis revealed two classes of *GFAP-Cre;* HIF2$\alpha^{flox/flox}$ mice at P10 (Fig. 7A; Supplemental Fig. S2). In the first class, astrocyte VEGF staining was almost entirely absent, demonstrating effective elimination of HIF2α function (Fig. 7A). These mice had reduced astrocyte numbers and lacked retinal vasculature (Fig. 7C and data not shown), consistent with previous findings using this same Cre line (Duan et al., 2014). In the second class of mutants, we were surprised to find that virtually all astrocytes continued to express VEGF (Fig. 7A). In these cases, retinal vasculature was present and astrocyte numbers were normal (Supplemental Fig. S2 and data not shown). This was unexpected because we and others have previously shown that this *GFAP-Cre* line drives Cre reporter activity in the vast majority of astrocytes as early as P1 (O'Sullivan et al., 2017; Puñal et al., 2019; Rattner et al., 2019). Virtually all P10 mice fell into either the "VEGF-high" or "VEGF-low" classes; we only observed one intermediate case where both VEGF$^+$ and VEGF$^-$ astrocytes were present. By contrast, at P2 we more often observed a mixture of VEGF$^+$ and VEGF$^-$ astrocytes. We therefore speculate that the VEGF-high cases arose because a minority of Cre-negative, HIF2α-positive astrocytes gained a proliferative advantage over their mutant neighbors and outcompeted them to colonize the retina. Regardless of the precise cause, it was clear that the VEGF-high class of animals did not in fact lack HIF2α function, so we excluded them from further analysis.

To test whether astrocyte HIF function mediates pathological proliferation, we exposed AC-Hif2α-KO mice and their littermate controls to the NOIR paradigm. Littermates included both HIF2$\alpha^{flox/flox}$ mice lacking the Cre transgene and *GFAP-Cre;* HIF2$\alpha^{+/+}$ mice, which were phenotypically indistinguishable; together we refer to them as HIF2α^{WT} animals. As in our previous experiments using CD-1 mice (Fig. 3), HIF2α^{WT} mice exposed to the NOIR protocol showed a dramatic increase in astrocyte numbers. By contrast, no such increase was observed in mice lacking astrocytic HIF2α function (Fig. 7B,C). These data strongly suggest that HIF2α is required within astrocytes to drive the proliferative response observed following return to room air at P4.

Discussion

In this study, we found that developing retinal astrocytes are sensitive to oxygen stress. Return to room air following a brief period of neonatal hyperoxia stimulated exuberant mitotic activity in retinal astrocytes, at an age when maturing astrocytes are normally ceasing their proliferation. Exposure to neonatal oxygen also perturbed retinal angiogenesis, with delays in peripheral vessel extension, persistent hyaloid vasculature, irregular and abnormally dense endothelial networks lacking regular capillary morphology, and associated vitreous hemorrhage. Within retinas, the severity of these vascular pathologies was correlated with the total number of astrocytes, suggesting that the two phenotypes may be linked. We propose a model in which neonatal hyperoxia recalibrates the baseline oxygen level sensed by astrocytes, such that return to room air triggers a HIF2α-dependent hypoxic response that includes astrocyte proliferation. Subsequently, excessive astrocyte numbers contribute to developmental retinal vasculopathy, including delayed peripheral extension, abnormal vascular patterning, hemorrhage, and, ultimately, retinal degenerative changes.

Neonatal hyperoxia alters the trajectory of retinal vascular development.

Consistent with previous reports (Claxton and Fruttiger, 2003; Morita et al., 2016; West et al., 2005), we found that hyperoxia from P0 prevented the initiation of retinal angiogenesis; only after return to normoxia did retinal vessels sprout from the ONH. Meanwhile, the embryonic hyaloid vascular system, which normally regresses in conjunction with elaboration of the intrinsic retinal vessels, persisted. Also similar to earlier reports (Claxton and Fruttiger, 2003; Morita et al., 2016; West et al., 2005), we found that starting hyperoxia at P0 has qualitatively different effects compared to later ages. Hyperoxia from P2 or P4 – ages in the mouse at which retinal vessels have sprouted from the ONH but

have not reached the retinal periphery – does not arrest peripheral extension, but instead causes central vaso-obliteration similar to P7-12 OIR (Smith et al., 1994). This observation suggests that initiation of retinal angiogenesis is a distinct and segregable process from peripheral extension of intraretinal vessels, and that each process responds differently to oxygen.

When retinal angiogenesis does eventually begin following return to room air, it is not only delayed but also disordered; retinas lacked normal capillary meshwork organization, with severe cases instead displaying dense sheets of endothelial cells without tubular structures. A primary vascular plexus was completed with variable delay, but with long-lasting retinal abnormalities including preretinal vascular membranes, retinal folds suggestive of tractional retinal detachments, reactive Müller glia, and vitreous hemorrhage. These findings differ from a recent study that exposed mice to P0-4 hyperoxia; in this study the effects on retinal vasculature were reported to be transient, correcting by P21 (Morita et al., 2016). The reason for this discrepancy is unclear, but since we observed persistent pathology only in ~50% of treated animals, one possibility is that the previous study did not use sufficient sample size to detect these effects. Our results are consistent with pathologies seen in young adult mice exposed to hyperoxia from P0-P7 (McMenamin et al., 2016). Together these findings suggest that initiation of hyperoxia earlier than the traditional OIR model (Smith et al., 1994) can produce a different vascular phenotype, with the vitreoretinopathy and tractional detachments potentially mirroring some aspects of ROP (Foos, 1987) that are not well modelled by OIR.

Retinal astrocyte proliferation is bidirectionally regulated by environmental oxygen

It has long been suspected that astrocytes might be sensitive to tissue hypoxia: Astrocytes are the key source of VEGF-A in the neonatal retina and have a key role in promoting angiogenesis (Rattner et al., 2019; Stone et al., 1995). Furthermore, the arrival of blood vessels at any given retinal location induces key features astrocyte maturation: VEGF expression is downregulated while GFAP and other mature markers become upregulated (Chan-Ling et al., 2009; West et al., 2005). These observations suggest that immature astrocytes have the capacity to detect oxygen levels and are a key part of the feedback loop that drives angiogenesis in response to hypoxia. However, it was unclear whether this capacity for oxygen sensing is used as a mechanism to control astrocyte development. A previous study addressing this question found only minor in vivo effects in rats exposed to hyperoxia (Zhang et al., 1999). Here we show that mitotic activity of neonatal astrocytes is bidirectionally regulated by oxygen – hyperoxia from P0-P4 suppresses proliferation while direct hypoxia promotes it. Our data are consistent with a model in which astrocytes sense local tissue oxygen levels using the HIF2α pathway, which drives

proliferation in a manner that is proportional to the amount of HIF signaling. Such a mechanism would serve retinal metabolic needs by ensuring the addition of more $VEGF^+$ angiogenic astrocytes when the tissue is hypoxic, and by suppressing this process once vessels have arrived to relieve this local hypoxia. Manipulations of environmental oxygen appear to disrupt this homeostatic mechanism, such that decrements from baseline oxygenation are sufficient to drive HIF activity and excessive astrocyte proliferation. Consistent with this idea, we observed that both absolute hypoxia (10% O_2) and normoxia following hyperoxia (dropping from 75% to 21% O_2) can stimulate astrocyte proliferation in a similar manner.

West et al. (2005) reported a seemingly contradictory result, in that astrocytes in hyperoxia-exposed retinas had higher rates of BrdU incorporation compared to normoxic controls. We suggest that different timelines of oxygen treatment could provide an explanation that reconciles the two studies: West et al. (2005) raised mice in 80% O_2 for 8 days before analyzing astrocytes, whereas our 75% O_2 manipulation ended at 4 days of age. During the first weeks of life, the mouse retina increases its metabolic activity as retinal waves and then light-responsive circuit activity begin (Ford and Feller, 2012). Consequently, an imbalance between oxygen supply and demand could develop by the end of the first postnatal week, leading to a state in which the tissue is hypoxic due to avascularity even while environmental oxygen is high. Indeed, the interpretation proposed by West et al. (2005) was that hypoxia – not hyperoxia – was driving the proliferation they observed.

It is likely that the pro-proliferative effect of hypoxia is limited to a brief period of astrocyte development, since no such proliferation has been reported following return to room air in the P7-12 OIR paradigm. By P7 retinal astrocytes are substantially more mature: They have completed migration, ceased proliferating, and assumed a mature GFAP-expressing molecular profile (Chan-Ling et al., 2009; O'Sullivan et al., 2017; West et al., 2005). It is plausible that mature astrocytes may respond differently to metabolic stresses. Furthermore, most retinal astrocytes reside in close contact with vasculature by P7 – another key change that could well contribute to the difference between the two hyperoxia paradigms.

Intrinsic astrocyte hypoxia signaling through HIF2α governs astrocyte abundance

Previous studies have reported conflicting results regarding the function of HIF2α within astrocytes. Duan et al. used *GFAP-Cre* mice either to stimulate the HIF pathway, through deletion of the negative regulator PHD2, or to suppress the pathway through deletion of HIF2α. These studies showed that activation increases astrocyte density while suppression reduces density, suggesting a possible role

for the HIF pathway in regulating astrocyte proliferation (Duan and Fong, 2019; Duan et al., 2014). On the other hand, another study using a different *GFAP-Cre* mouse failed to find any effect of astrocytic Hif2α deletion (Weidemann et al., 2010). One possible explanation for this discrepancy is that the efficacy of the *GFAP-Cre*-mediated gene deletion might be variable. For this reason, we decided to monitor HIF pathway activity in our AC-Hif2α-KO mice by staining for VEGF-A, a known HIF target gene. Using this strategy, we validated that the *GFAP-Cre* line used in the two Duan studies (Zhuo et al., 2001) does indeed abrogate HIF function, at least in a subset of AC-Hif2α-KO mice. The VEGF-low mutants exhibited the same phenotype reported by Duan et al. (2014) – i.e. decreases in astrocyte abundance and failure of retinal angiogenesis. Moreover, exposing these mutants to a strong pro-mitotic stimulus – i.e. relative hypoxia via the NOIR paradigm – failed to expand the astrocyte population, further supporting the notion that astrocyte proliferation does indeed require HIF signaling. Our replication of the vascular phenotype is in accordance with recent work – again using the same Cre line – showing that astrocyte-derived VEGF-A is essential for initiation of angiogenesis (Rattner et al., 2019). Overall these results support the notion that astrocyte HIF2α is required both for 1) retinal angiogenesis via induction of VEGF, and 2) hypoxia-induced astrocyte proliferation. The mechanism by which HIF2α promotes proliferation will be an interesting topic for future studies.

Our VEGF staining also revealed a subset of AC-Hif2α-KO mice in which cells retaining HIF function had apparently taken over the astrocyte population. We suggest that this likely occurred in animals where *GFAP-Cre* recombination did not go to completion in all astrocytes. In this case, Cre^{-} astrocyte precursors retaining HIF function might have been at a competitive advantage relative to Cre^{+} mutant cells, particularly if the HIF pathway is required for astrocyte proliferation (Duan et al., 2014; Fig. 7). These results highlight a potential source of confusion for past studies of HIF and VEGF in astrocytes, and accentuate the need to validate knockout efficacy when genes affecting proliferation are targeted.

Role of astrocytes in oxygen-induced vasculopathy

Our results from the NOIR paradigm show a strong correlation between the magnitude of astrocyte overproduction and the severity of the vascular delay and disarray. Since astrocyte phenotypes precede vessel growth and occur in peripheral retina prior to the arrival of vessels, we favor a model in which hyperoxia affects astrocytes, and astrocytes in turn contribute to pathologic retinal vascularization. This would be consistent with other manipulations of astrocyte population size during development, each of which demonstrate that vascular development is highly sensitive to the number of astrocytes within the angiogenic template (Duan and Fong, 2019; Fruttiger et al., 1996; O'Sullivan et

al., 2017; Puñal et al., 2019; Tao and Zhang, 2016). However, our experiments cannot exclude the possibility of additional factors explaining the correlation between astrocytic and vascular phenotypes. Furthermore, additional astrocyte abnormalities may well arise as a result of vascular development errors, given that astrocytes depend on signals from endothelial cells for their own maturation (Mi et al., 2001; Sakimoto et al., 2012; Selvam et al., 2018). Further work will be required to better elucidate the mechanisms by which astrocytes and endothelial cells interact during development and disease.

Implications for ROP

Several of the defining features of ROP, such as delayed peripheral vascularization, astrocyte hyperproliferation, and long-lasting retinopathy have been challenging to model in the mouse and are absent in the classic P7-P12 mouse OIR model (Gariano, 2010). The neontatal hyperoxia paradigm we employed here and recently by other groups (McMenamin et al., 2016; Morita et al., 2016) thus has several phenotypic features that make it a useful complement to the traditional mouse OIR. First, the astrocyte hyperproliferation phenotype we describe in this study could provide useful insight into formation of the astrocyte-dense fibrovascular ridge that forms in the mid-periphery of ROP retinas (Foos, 1987). Additionally, the enduring retinopathy produced by neonatal hyperoxia – rather than the spontaneously resolving vaso-obliteration and neovascularization in OIR – could provide valuable developmental outcome measures for potential therapies.

Current treatment strategies for ROP target “Phase 2” and aim to reduce neovascularization either by 1) ablating ischemic peripheral retina to eliminate the source of abnormal proangiogenic signals or 2) blocking VEGF signaling. While overall helpful in preserving functional vision in affected children, both approaches intervene relatively late in the pathogenesis of ROP and aim to suppress angiogenesis. Additionally, laser and cryoablation are inherently destructive procedures, and concerns remain regarding possible ocular and systemic side effects of anti-VEGF therapy during development. Better understanding the pathogenesis of ROP and the role of astrocytes could reveal new targets for treating or preventing retinal vascular disorders. Our results suggest that inhibiting astrocyte overproliferation could be a promising therapeutic avenue, although it is likely this will need to be done in a HIF-independent manner given the essential role of the HIF- VEGF axis in driving angiogenesis (Duan et al., 2014; Rattner et al., 2019).

Conclusions

In this study, we report that neonatal hyperoxia in mice primes retinal astrocytes to respond to normoxia with an abnormal surge in mitotic activity. The hyperproliferation in this context resembles the response of astrocytes to hypoxia and depends on the canonical hypoxia-signaling molecule HIF2α, suggesting that relative hypoxia is the physiologic stimulus for cell division in both cases. In retinas following neonatal hyperoxia exposure, angiogenesis is defective and eyes are prone to vitreous hemorrhage and degenerative changes reminiscent of advanced ROP. We propose a model in which oxygen instability produces excessive numbers of immature astrocytes in the developing retina, and quantitative and qualitative defects in the astrocyte network contribute to delayed and disordered retinal vascularization. These findings suggest that astrocytes could play a role in mediating the pathobiology of ROP.

Acknowledgements

This work was supported by the National Eye Institute (EY030611 to J.N.K; EY5722 to Duke University); the Ruth K. Broad Foundation (J.N.K.); Research to Prevent Blindness (Unrestricted Grant to Duke University); and a Duke University Holland-Trice award (J.N.K.). We thank Ari Pereira for mouse husbandry; William Marcus for technical assistance; and William Spencer for help with photography. The funders had no role in study design, data collection and analysis, decision to publish, or preparation of the manuscript.

Competing Interest

The authors declare no competing interests.

References

Chan-Ling, T., Chu, Y., Baxter, L., Weible Ii, M. and Hughes, S. (2009). In vivo characterization of astrocyte precursor cells (APCs) and astrocytes in developing rat retinae: differentiation, proliferation, and apoptosis. *Glia* **57**, 39–53.

Claxton, S. and Fruttiger, M. (2003). Role of arteries in oxygen induced vaso-obliteration. *Exp. Eye Res.* **77**, 305–11.

Dorrell, M. I., Aguilar, E. and Friedlander, M. (2002). Retinal vascular development is mediated by endothelial filopodia, a preexisting astrocytic template and specific R-cadherin adhesion. *Invest. Ophthalmol. Vis. Sci.* **43**, 3500–10.

Duan, L.-J. and Fong, G.-H. (2019). Developmental vascular pruning in neonatal mouse retinas is programmed by the astrocytic oxygen-sensing mechanism. *Development* **146**, dev175117.

Duan, L.-J., Takeda, K. and Fong, G.-H. (2014). Hypoxia inducible factor-2α regulates the development of retinal astrocytic network by maintaining adequate supply of astrocyte progenitors. *PLoS One* **9**, e84736.

Eller, A. W., Jabbour, N. M., Hirose, T. and Schepens, C. L. (1987). Retinopathy of prematurity. The association of a persistent hyaloid artery. *Ophthalmology* **94**, 444–8.

Foos, R. Y. (1987). Retinopathy of prematurity. Pathologic correlation of clinical stages. *Retina* **7**, 260–76.

Fruttiger, M. (2002). Development of the mouse retinal vasculature: angiogenesis versus vasculogenesis. *Invest. Ophthalmol. Vis. Sci.* **43**, 522–7.

Fruttiger, M., Calver, A. R., Krüger, W. H., Mudhar, H. S., Michalovich, D., Takakura, N., Nishikawa, S. and Richardson, W. D. (1996). PDGF mediates a neuron-astrocyte interaction in the developing retina. *Neuron* **17**, 1117–31.

Gariano, R. F. (2010). Special features of human retinal angiogenesis. *Eye (Lond).* **24**, 401–7.

Gerhardt, H., Golding, M., Fruttiger, M., Ruhrberg, C., Lundkvist, A., Abramsson, A., Jeltsch, M., Mitchell, C., Alitalo, K., Shima, D., et al. (2003). VEGF guides angiogenic sprouting utilizing endothelial tip cell filopodia. *J. Cell Biol.* **161**, 1163–1177.

Gruber, M., Hu, C.-J., Johnson, R. S., Brown, E. J., Keith, B. and Simon, M. C. (2007). Acute postnatal ablation of Hif-2 results in anemia. *Proc. Natl. Acad. Sci.* **104**, 2301–2306.

Hellström, A., Smith, L. E. H. and Dammann, O. (2013). Retinopathy of prematurity. *Lancet (London, England)* **382**, 1445–57.

Kurihara, T., Kubota, Y., Ozawa, Y., Takubo, K., Noda, K., Simon, M. C., Johnson, R. S., Suematsu, M., Tsubota, K., Ishida, S., et al. (2010). von Hippel-Lindau protein regulates transition from the fetal to the adult circulatory system in retina. *Development* **137**, 1563–71.

Lajko, M., Cardona, H. J., Taylor, J. M., Shah, R. S., Farrow, K. N. and Fawzi, A. A. (2016). Hyperoxia-Induced Proliferative Retinopathy: Early Interruption of Retinal Vascular Development with Severe and Irreversible Neurovascular Disruption. *PLoS One* **11**, e0166886.

McMenamin, P. G., Kenny, R., Tahija, S., Lim, J., Naranjo Golborne, C., Chen, X., Bouch, S., Sozo, F. and Bui, B. (2016). Early Postnatal Hyperoxia in Mice Leads to Severe Persistent Vitreoretinopathy. *Invest. Ophthalmol. Vis. Sci.* **57**, 6513–6526.

Mi, H., Haeberle, H. and Barres, B. A. (2001). Induction of astrocyte differentiation by endothelial cells. *J. Neurosci.* **21**, 1538–47.

Morita, A., Ushikubo, H., Mori, A., Sakamoto, K. and Nakahara, T. (2016). Exposure to High-Concentration Oxygen in the Neonatal Period Induces Abnormal Retinal Vascular Patterning in Mice. *Birth Defects Res. B. Dev. Reprod. Toxicol.* 1–9.

Mowat, F. M., Luhmann, U. F. O., Smith, A. J., Lange, C., Duran, Y., Harten, S., Shukla, D., Maxwell, P. H., Ali, R. R. and Bainbridge, J. W. B. (2010). HIF-1alpha and HIF-2alpha Are Differentially Activated in Distinct Cell Populations in Retinal Ischaemia. *PLoS One* **5**, e11103.

Nakamura-Ishizu, A., Kurihara, T., Okuno, Y., Ozawa, Y., Kishi, K., Goda, N., Tsubota, K., Okano, H., Suda, T. and Kubota, Y. (2012). The formation of an angiogenic astrocyte template is regulated by the neuroretina in a HIF-1-dependent manner. *Dev. Biol.* **363**, 106–14.

O'Sullivan, M. L., Puñal, V. M., Kerstein, P. C., Brzezinski, J. A., Glaser, T., Wright, K. M. and

Kay, J. N. (2017). Astrocytes follow ganglion cell axons to establish an angiogenic template during retinal development. *Glia* **65**, 1697–1716.

Pagès, G. and Pouysségur, J. (2005). Transcriptional regulation of the Vascular Endothelial Growth Factor gene - A concert of activating factors. *Cardiovasc. Res.* **65**, 564–573.

Puñal, V. M., Paisley, C. E., Brecha, F. S., Lee, M. A., Perelli, R. M., Wang, J., O'Koren, E. G., Ackley, C. R., Saban, D. R., Reese, B. E., et al. (2019). Large-scale death of retinal astrocytes during normal development is non-apoptotic and implemented by microglia. *PLoS Biol.* **17**, e3000492.

Rattner, A., Williams, J. and Nathans, J. (2019). Roles of HIFs and VEGF in angiogenesis in the retina and brain. *J. Clin. Invest.* **130**, 3807–3820.

Sakimoto, S., Kidoya, H., Naito, H., Kamei, M., Sakaguchi, H., Goda, N., Fukamizu, a, Nishida, K. and Takakura, N. (2012). A role for endothelial cells in promoting the maturation of astrocytes through the apelin/APJ system in mice. *Development* **139**, 1327–1335.

Schindelin, J., Arganda-Carreras, I., Frise, E., Kaynig, V., Longair, M., Pietzsch, T., Preibisch, S., Rueden, C., Saalfeld, S., Schmid, B., et al. (2012). Fiji: an open-source platform for biological-image analysis. *Nat. Methods* **9**, 676–82.

Selvam, S., Kumar, T. and Fruttiger, M. (2018). Retinal vasculature development in health and disease. *Prog. Retin. Eye Res.* **63**, 1–19.

Smith, L. E., Wesolowski, E., McLellan, A., Kostyk, S. K., D'Amato, R., Sullivan, R. and D'Amore, P. A. (1994). Oxygen-induced retinopathy in the mouse. *Invest. Ophthalmol. Vis. Sci.* **35**, 101–11.

Stone, J., Itin, A., Alon, T., Pe'er, J., Gnessin, H., Chan-Ling, T. and Keshet, E. (1995). Development of retinal vasculature is mediated by hypoxia-induced vascular endothelial growth factor (VEGF) expression by neuroglia. *J. Neurosci.* **15**, 4738–47.

Sun, Y., Dalal, R. and Gariano, R. F. (2010). Cellular composition of the ridge in retinopathy of prematurity. *Arch. Ophthalmol. (Chicago, Ill. 1960)* **128**, 638–41.

Tao, C. and Zhang, X. (2016). Retinal Proteoglycans Act as Cellular Receptors for Basement Membrane Assembly to Control Astrocyte Migration and Angiogenesis. *Cell Rep.* **17**, 1832–1844.

Weidemann, A., Krohne, T. U., Aguilar, E., Kurihara, T., Takeda, N., Dorrell, M. I., Simon, M. C., Haase, V. H., Friedlander, M. and Johnson, R. S. (2010). Astrocyte hypoxic response is essential for pathological but not developmental angiogenesis of the retina. *Glia* **58**, 1177–85.

West, H., Richardson, W. D. and Fruttiger, M. (2005). Stabilization of the retinal vascular network by reciprocal feedback between blood vessels and astrocytes. *Development* **132**, 1855–62.

Zhang, Y., Porat, R. M., Alon, T., Keshet, E. and Stone, J. (1999). Tissue oxygen levels control astrocyte movement and differentiation in developing retina. *Brain Res. Dev. Brain Res.* **118**, 135–45.

Zhuo, L., Theis, M., Alvarez-Maya, I., Brenner, M., Willecke, K. and Messing, A. (2001). hGFAP-cre transgenic mice for manipulation of glial and neuronal function in vivo. *Genesis* **31**, 85–94.

Figures and Legends

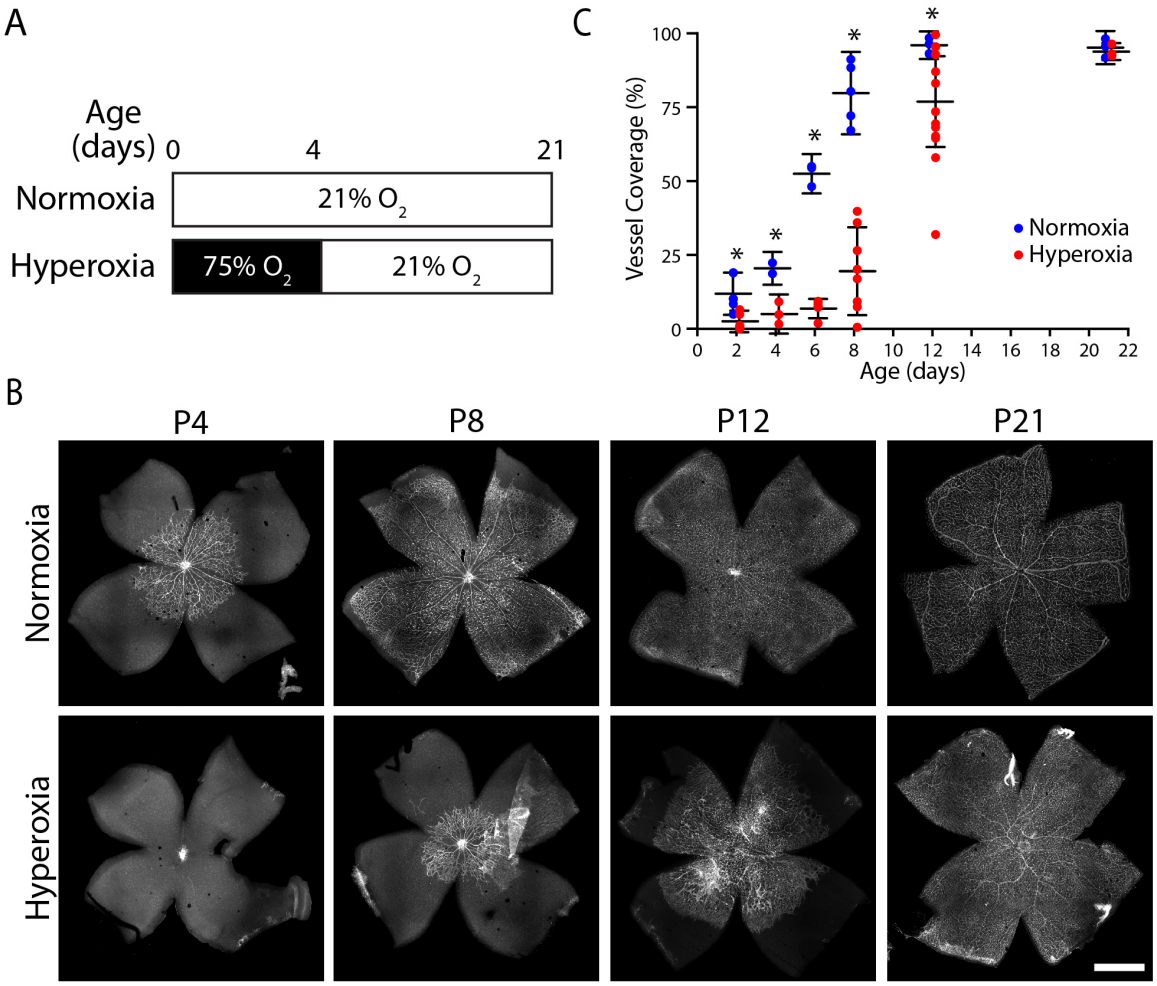

Figure 1. Neonatal hyperoxia prevents retinal angiogenesis

A) Schematic of experimental timeline. *Control* animals were maintained in room air (21% O_2) throughout; *Hyperoxia* animals were raised in 75% O_2 from P0-P4 before returning to room air (21% O_2) at P4. **B**) Example confocal images of IB4-stained flat-mounted retinas, showing retinal vasculature. Images are stitched composites of individual 20x tiles. In normoxia controls, angiogenesis is initiated shortly after birth and the inner retinal surface is completely vascularized by P12. In the hyperoxia condition, angiogenesis is completely prevented until animals are returned to room air at P4. Scale bar: 1 mm. **C**) Summary data of retinal vascular area by condition for animals sacrificed at different ages. There was a significant angiogenic delay in hyperoxia animals. Statistics: Two-way ANOVA. Main effect of age $F(5,50) = 82.6$, $p < 0.0001$; main effect of oxygen $F(1,50) = 55.7$, $p < 0.0001$; interaction, $F(5,50) = 9.4$, $p < 0.0001$.). Asterisks denote significant differences by Holm-Sidak multiple comparisons test ($P < 0.05$).

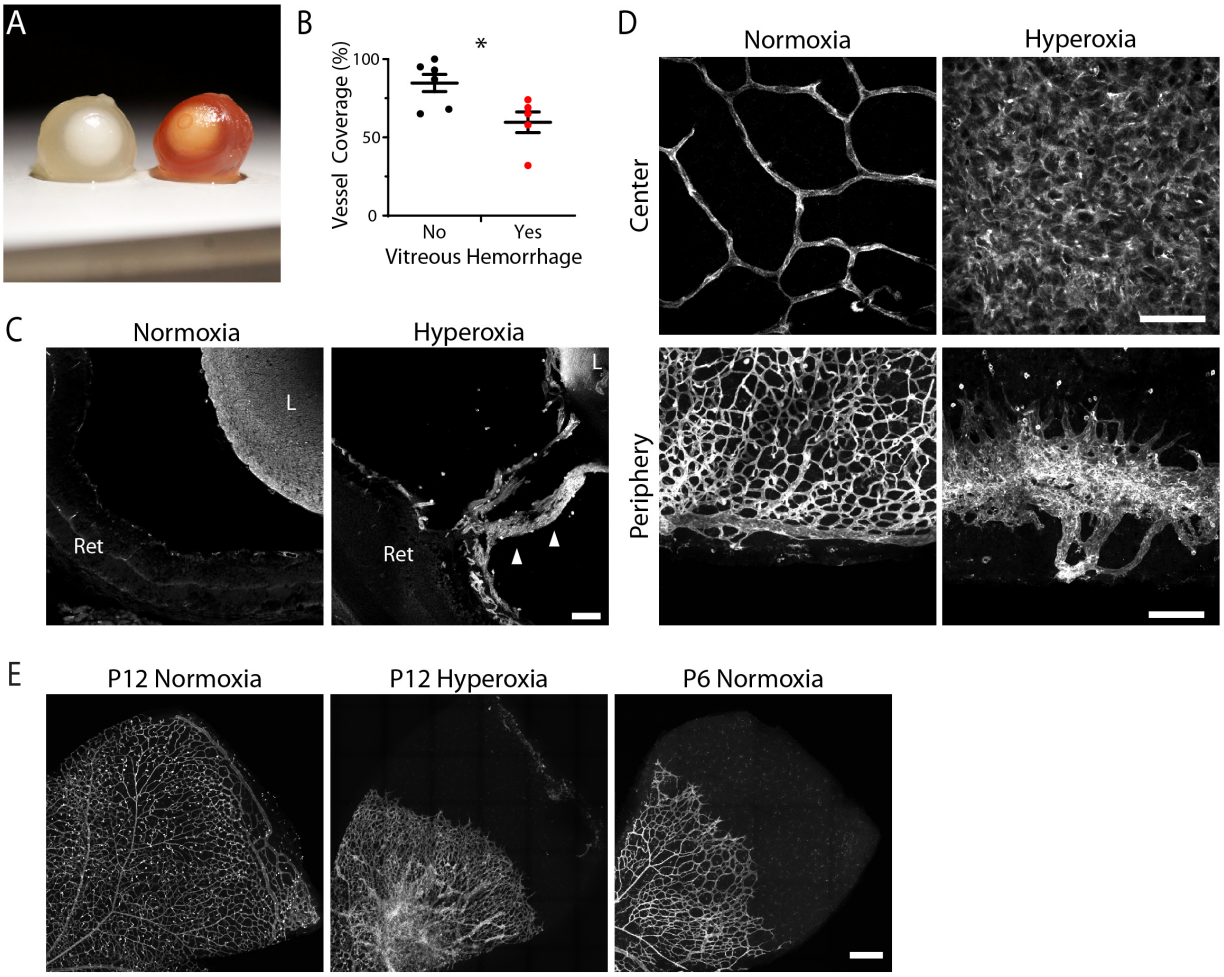

Figure 2. Angiogenesis is abnormal following return to room air in NOIR protocol.

A) Photographs of freshly dissected P10 eyes from P0-P4 hyperoxia treated mice, showing examples of globes with gross vitreous hemorrhage (right) and without hemorrhage (left). **B**) Percentage of retinal area inside vessel wavefront in P12 NOIR retinas. Animals grouped by presence or absence of vitreous hemorrhage. **C**) Central retina region from P10 whole-eye cryosections stained with IB4 to reveal vasculature. Hyaloid vessels (arrows) traversing space between retina (Ret) and lens (L) are retained in hyperoxia but not control animals. **D**) Example en-face confocal images of IB4-stained P12 retinas. Images are Z-projections of stacks encompassing the nerve fiber layer. Controls (left) show mature capillary network in central retina, and complete primary plexus in the periphery with terminal circumferential vessel. Hyperoxia animals (right) show lawn of endothelial cells lacking capillary morphology in central retina, and periphery with IB4+ ring of vitreous-derived vascular tissue not connected to intrinsic retinal vessels. **E**) Low magnification en-face images illustrating vascular

disorganization in hyperoxia treated mice. Images are oriented with ONH down and left. In P12 control, complete primary plexus is organized with large radial vessels giving rise to capillary network. P12 hyperoxia retina exhibits peripheral avascular zone, absence of large radial vessels, and hyperdense and irregular vascularity centrally. P6 control retina in which the vascular wavefront is at a similar eccentricity demonstrating that the P12 hyperoxia morphology does not resemble a more immature stage. Statistics in B, two-tailed T test (No hemorrhage, 84.7 ± 5.5% vascular coverage, n = 6; vitreous hemorrhage, 59.6 ± 6.6%, n = 5; P = 0.026). Scale bars: C 100 μm; D top 50 μm; C bottom 150 μm; E 250 μm.

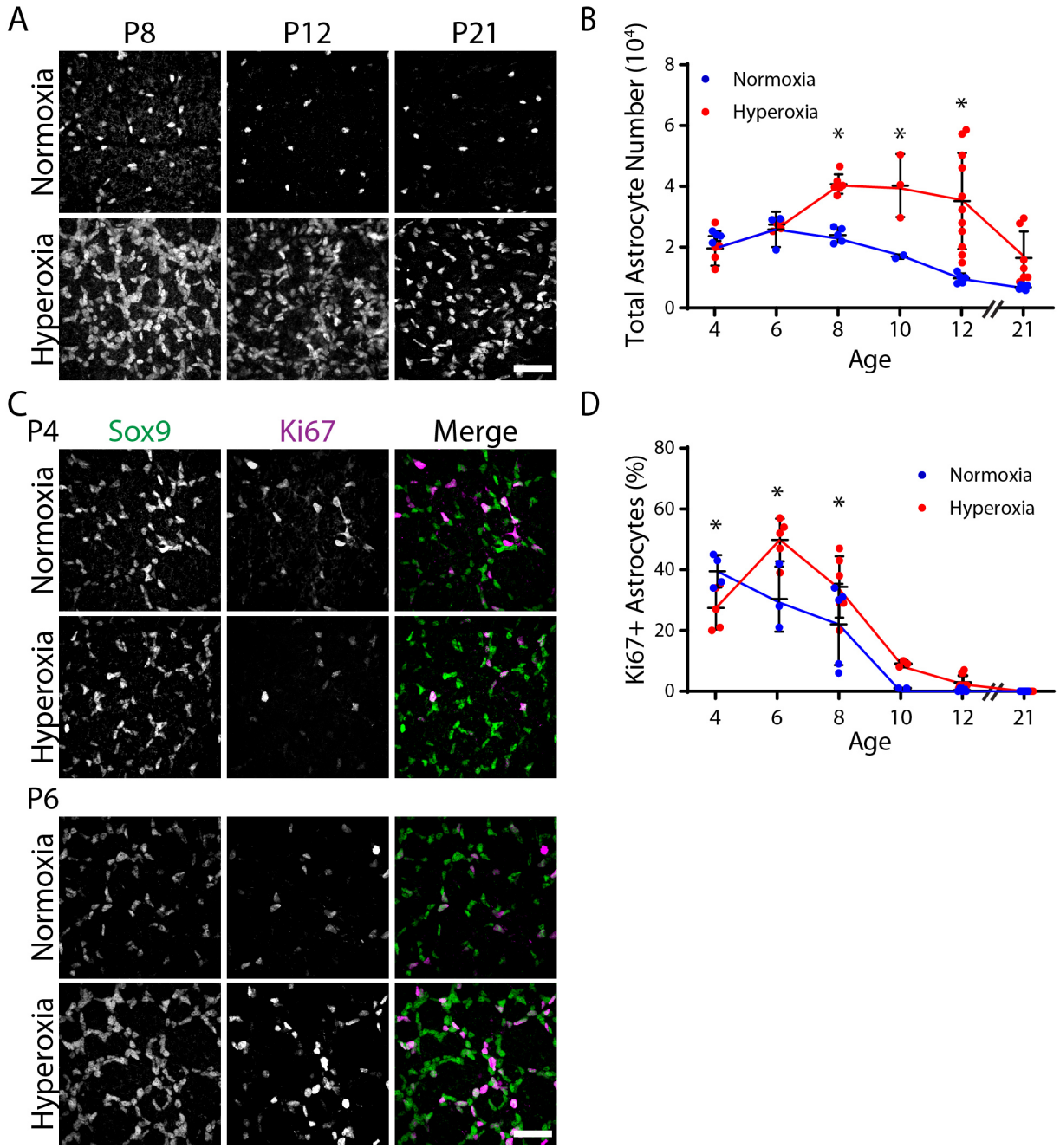

Figure 3. Astrocyte proliferation is suppressed by hyperoxia and stimulated by return to room air. **A**) Example en-face confocal images of the specific astrocyte nuclear marker Sox9. Hyperoxia treated retinas show significantly denser astrocytes. **B**) Summary of total astrocyte numbers calculated from quantification of images such as those shown in (A). From P8 to P12, hyperoxia exposed retinas had significantly more astrocytes than controls. At P21 there was not a group difference but some individual hyperoxia animals have nearly triple the number of astrocytes as controls. **C**) Example en-face images

of Sox9 and Ki67 double-stained retina. Ki67 marks mitotically active cells. Double-positive cells were counted as dividing astrocytes. At P4, the percentage of mitotically active astrocytes was reduced in hyperoxia retinas compared to controls, whereas at P6-8 after return to normoxia more astrocytes were actively dividing compared to controls. Statistics, two-way ANOVA. B: Main effect of age $F(5,46) = 11.67$, $p < 0.0001$; main effect of oxygen $F(1,46) = 29.85$, $p < 0.0001$; interaction, $F(5,46) = 4.999$, $p = 0.001$. D: Main effect of age $F(5,49) = 74.5$, $p < 0.0001$; main effect of oxygen $F(1,49) = 7.9$, $p = 0.007$; interaction, $F(5,49) = 6.336$, $p = 0.0001$. Asterisks denote significant differences by Holm-Sidak post-hoc test. P-values in B: P8 $P = 0.082$; P10 $P = 0.0136$. P12 $P < 0.0001$. P-values in D: P4 $P = 0.0268$; P6 $P = 0.0007$; P8 $P = 0.0122$. Scale bars 50 μm.

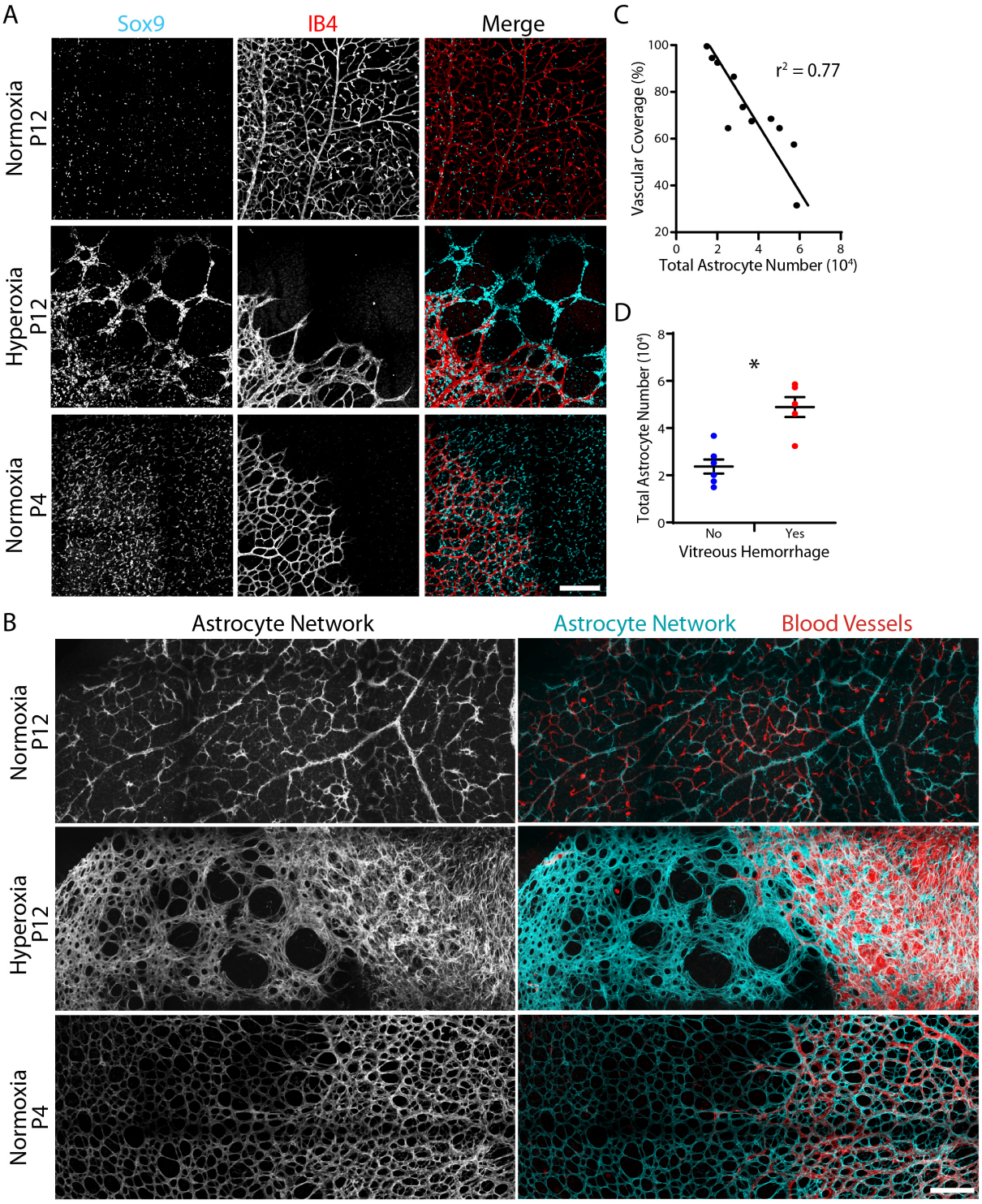

Figure 4. Astrocyte patterning is abnormal after hyperoxia.

A) Representative en-face confocal images of midperipheral retina stained with Sox9 and IB4 to label astrocyte nuclei and vasculature. **B**) Representative en-face images of astrocyte arbors, revealed by

anti-GFAP (P12) or anti-PDGFRα (P4). In P12 controls, astrocytes are homogenously distributed and evenly spaced across the retina (A,B). In P12 hyperoxia retinas, astrocyte somata are aggregated in clumps and strings in advance of the delayed vascular wavefront (A). Uneven patterning of the astrocyte arbor network is also evident (B). Despite these patterning defects, advancing endothelial cells remain associated with astrocytes, and do not enter astrocyte-free retinal regions (A,B). Blood vessels have reached a similar eccentricity in P4 controls, but astrocytes are evenly distributed rather than displaying the aggregation seen in hyperoxia retinas (A). The P4 arbor network is also far more uniform than in P12 treated animals (B). **C**) In P12 hyperoxia treated retinas, retinal vascular coverage is inversely correlated with the total number of astrocytes. **D**) Hyperoxia retinas with vitreous hemorrhages (e.g. Fig. 2A) have significantly more astrocytes than hyperoxia retinas without hemorrhage. Statistics, two-tailed T test; no hemorrhage, 23,721 ± 2,982 total astrocytes, n = 6; vitreous hemorrhage, 48,895 ± 4,220, n = 5; p = 0.0015. Scale bars 200 μm.

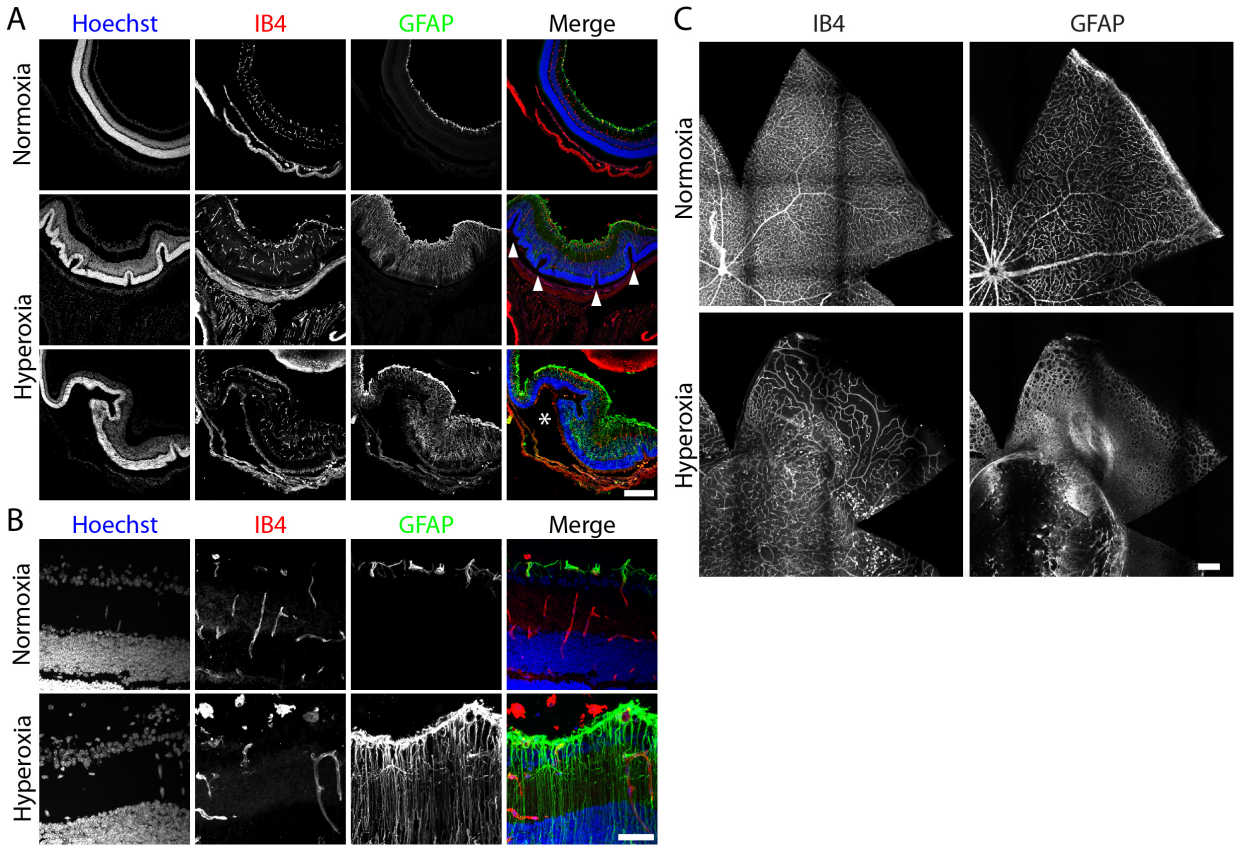

Figure 5. Neonatal hyperoxia causes enduring retinopathy.

A,B) Retinal cross-sections from P21 mice illustrating pathological features caused by P0-P4 hyperoxia. Low (A) and high (B) magnification representative confocal images of control or hyperoxia tissue stained for vasculature (IB4) or GFAP. Two examples of different hyperoxia retinas are given in A. Controls display regular laminar organization with smooth contours. GFAP staining is restricted to inner retina where astrocytes reside in the RNFL. Hyperoxia retinas are thickened; show ROP-like outer retinal folding (arrowheads; Foos, 1987); and express GFAP throughout the full depth of the retina indicating reactive Müller gliosis. Asterisk indicates large subretinal space underlying folded neuroretina suggestive of retinal detachment. B) Higher magnification view shows vitreal $IB4^+$ neovascular clumps, and radial distribution of GFAP staining in hyperoxia retinas consistent with Müller glia labeling. **C**) En-face view of vascular (IB4) and glial (GFAP) phenotypes at P21. Scale bars: A,C) 250 μm; B) 50 μm.

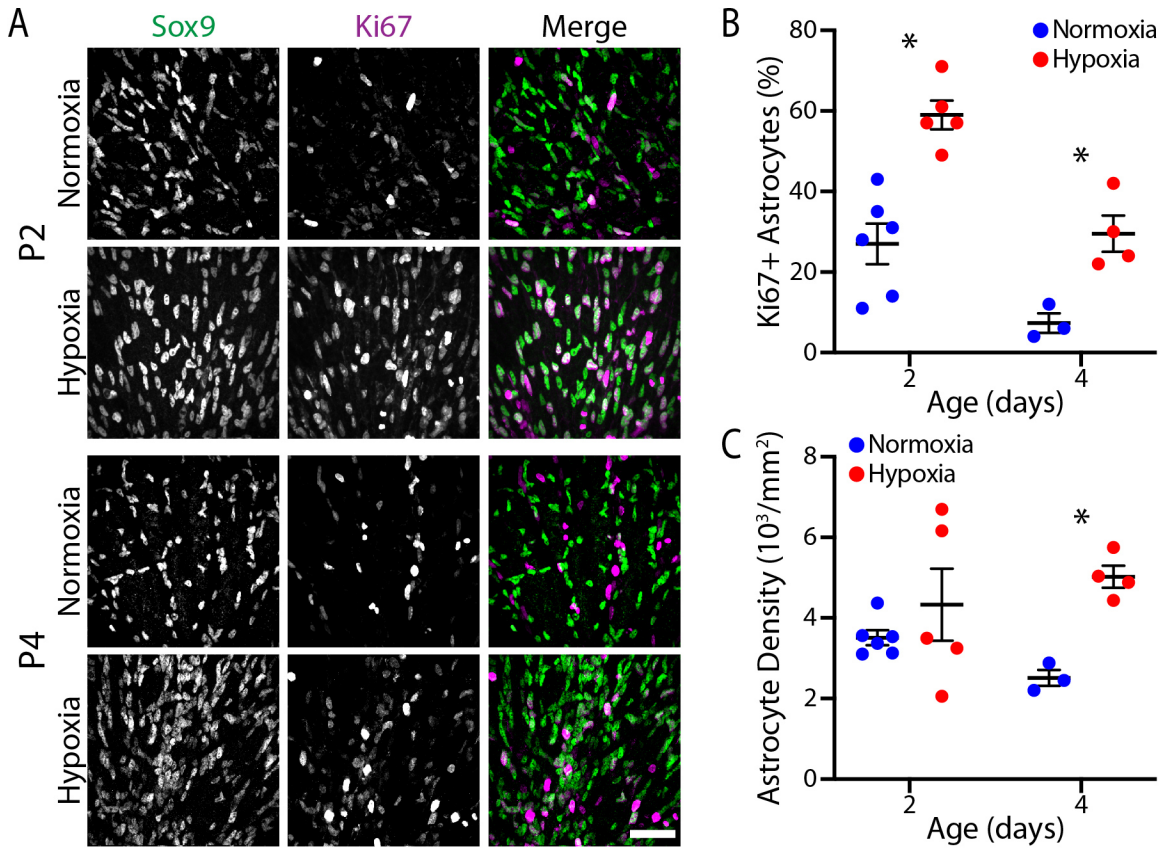

Figure 6. Hypoxia stimulates astrocyte proliferation.

A) En-face confocal images showing co-labeling for Sox9 and Ki67 in animals exposed to 10% hypoxia from birth, or their littermate controls. Representative examples are shown at P2 and P4. **B**) Effects of hypoxia on astrocyte proliferation were quantified from images similar to A, by calculating the fraction of astrocytes that expressed Ki67. Astrocyte proliferation was higher at both P2 and P4 in treated mice. **C**) Effects of hypoxia on astrocyte abundance, calculated from images similar to A. Astrocyte density became higher by P4 in treated animals. Statistics: Two-way ANOVA. B: Main effect of age $F(1,14) = 27.49$, $p = 0.0001$; main effect of oxygen $F(1,14) = 33.37$, $p < 0.0001$; interaction, $F(1,14) = 1.10$, $p = 0.3121$. C: Main effect of age $F(1,14) = 0.07$, $p = 0.7885$; main effect of oxygen $F(1,14) = 9.00$, $p = 0.0095$; interaction, $F(1,14) = 2.32$, $p = 0.1502$. Asterisks denote significant differences by post-hoc Holm-Sidak test. B: P2 P = 0.0002; P4 P = 0.0184. C: P2 P = 0.4434; P4 P = 0.0238. Scale bar, 50 µm.

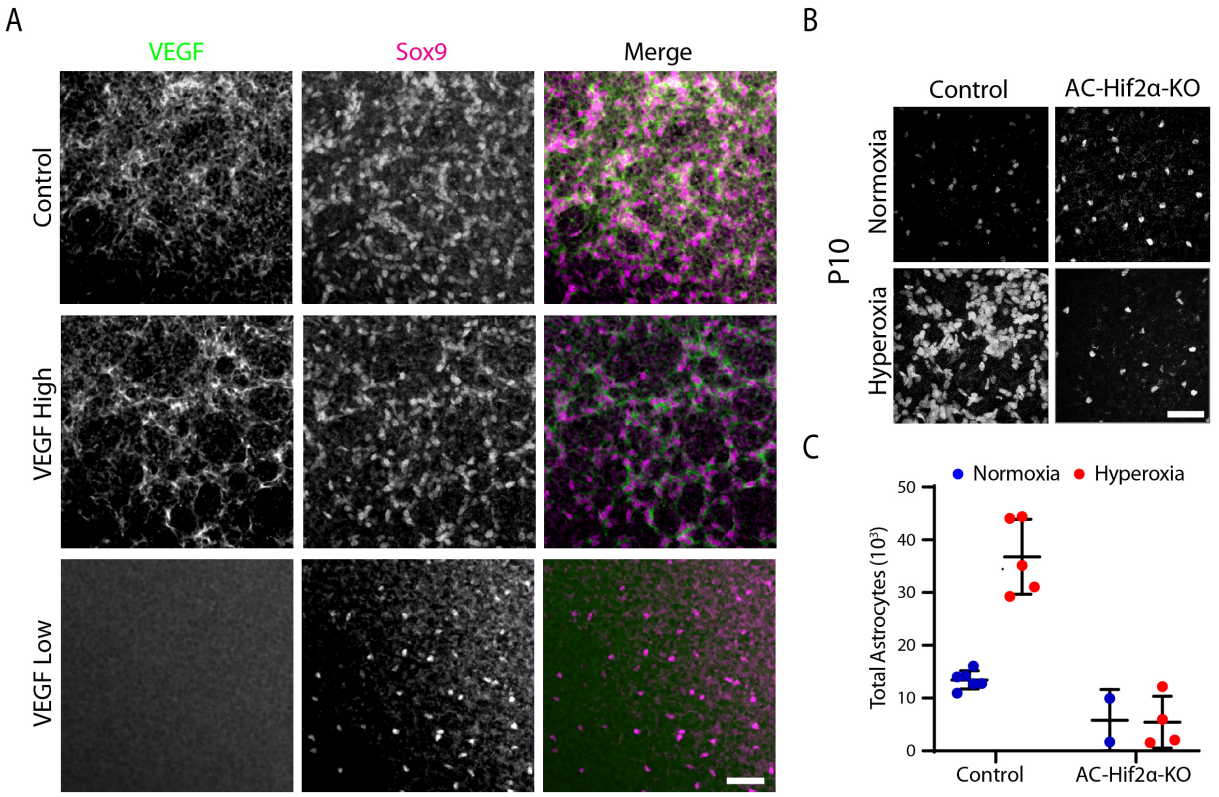

Figure 7. Astrocyte HIF2α is required for proliferation on return to room air in NOIR paradigm

A) Characterization of HIF pathway activation in astrocyte-specific *GFAP-Cre;* Hif2α^{flox} mutants (AC-Hif2α-KO). Representative en-face views of P10 retinas stained for astrocyte marker Sox9 and for anti-VEGF-A, a marker of HIF pathway activation. HIF2α^{WT} littermate controls (top row) show substantial astrocytic expression of VEGF in the NOIR paradigm. VEGF immunoreactivity is largely localized to Sox9^{+} cells and their arbors. In AC-Hif2α-KO mutants, we observed two phenotypic classes denoted VEGF High and VEGF Low. The first class (center row) exhibited VEGF staining indistinguishable from controls, suggesting a failure of HIF2α gene deletion. These were excluded from further analysis. VEGF Low mutants (bottom row) entirely lacked VEGF expression indicating successful abrogation of HIF signaling. **B,C**) Effects of the NOIR paradigm on P10 astrocyte numbers in AC-Hif2α-KO mice. B, representative Sox9 images; C, quantification of total Sox9^{+} astrocytes. Astrocyte numbers were greatly increased following hyperoxia in littermate controls, but not in AC-Hif2α-KO mutants. Scale bars, 50 µm.

Supplemental Figures and Legends

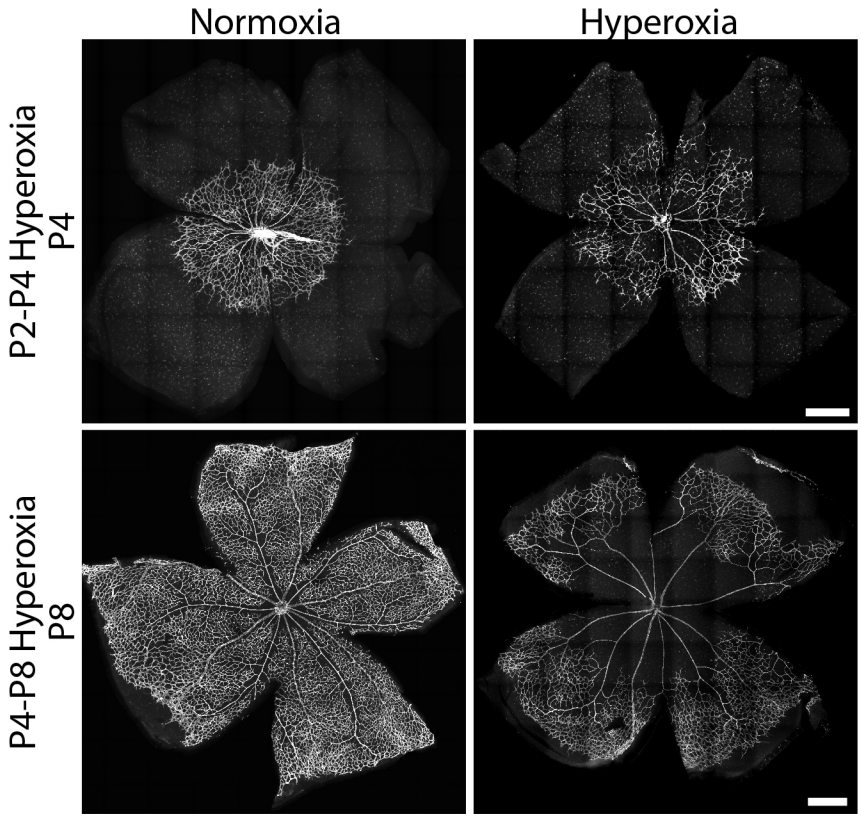

Figure S1. Effects of starting hyperoxia at P2 or P4. Representative whole-mount images of retinal vasculature from animals reared in 75% O_2 from P2-P4 (top) or P4-P8 (bottom). Progression of vascular wavefront is similar to normoxic littermate controls in both treatment paradigms. However, central vaso-obliteration is observed in treated animals, similar to standard P7-P12 OIR paradigm.

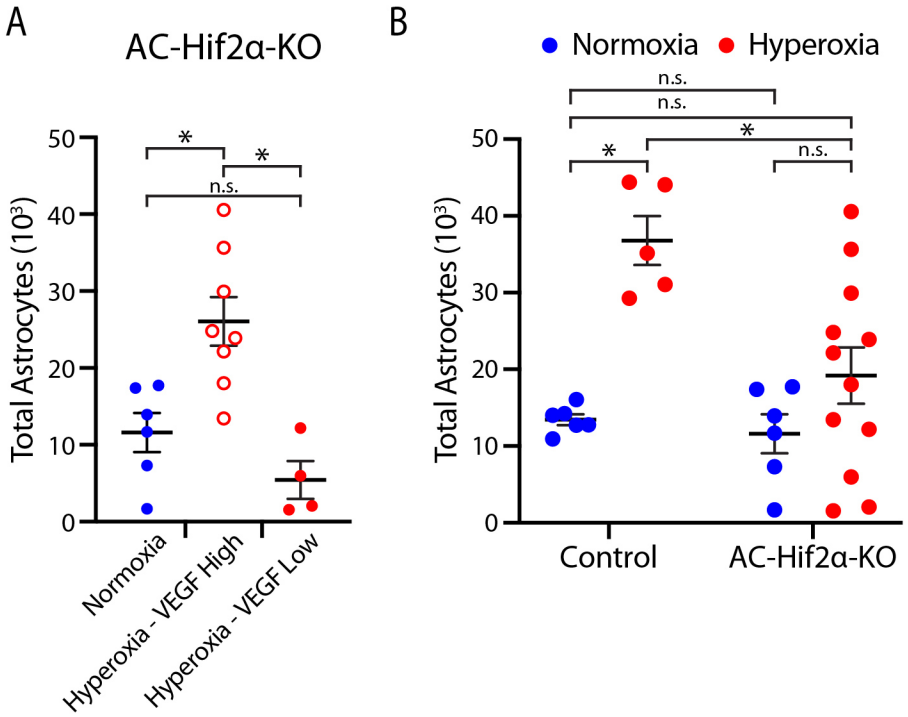

Figure S2. Further characterization of VEGF-High and VEGF-Low classes of Hif2α mutants. **A**) VEGF High and VEGF Low mutants (P10) have significantly different astrocyte production responses following hyperoxia treatment. One-way ANOVA with Tukey's post-hoc test, P = 0.0011. Normoxia vs. VEGF-high mutant, P = 0.0070. Normoxia vs. VEGF-low mutant, P = 0.4230. This finding provides further evidence that the two classes of mutants are fundamentally different and should be considered different experimental groups. **B**) Total astrocyte numbers at P10 in mutants and littermate controls. Graph is the same as Fig. 7C, except that all AC-Hif2α-KO mutants have been plotted regardless of VEGF status. Even when no distinction is made between mutants based on VEGF expression, there is still a significant effect of genotype on astrocyte number (Two-way ANOVA, main effect of genotype $F(1,25) = 7.02$, $p = 0.0138$; main effect of oxygen $F(1,25) = 17.75$, $p = 0.0003$; interaction, $F(1,25) = 4.626$, $p = 0.0414$). Furthermore, a post-hoc test (Holm-Sidak) shows that loss of Hif2α significantly blunts the effect of hyperoxia even when VEGF-high animals are included in the analysis (Holm-Sidak test, control hyperoxia vs. mutant hyperoxia, P = 0.0095). Consistent with this finding, we did not detect a significant astrocyte number difference between normoxic and hyperoxic mutants under these conditions (Holm-Sidak, P = 0.5287). Therefore, even though there is strong biological justification for excluding VEGF High mutants from the experiment, failing to do so does not change our central conclusion that Hif2α is required for the astrocyte proliferative response in the NOIR paradigm.